



**HAL**  
open science

## An experimental study of failure initiation and propagation in 2D woven composites under compression

N.V. de Carvalho, S.T. Pinho, P. Robinson

### ► To cite this version:

N.V. de Carvalho, S.T. Pinho, P. Robinson. An experimental study of failure initiation and propagation in 2D woven composites under compression. *Composites Science and Technology*, 2011, 71 (10), pp.1316. 10.1016/j.compscitech.2011.04.019 . hal-00768854

**HAL Id: hal-00768854**

**<https://hal.science/hal-00768854v1>**

Submitted on 26 Dec 2012

**HAL** is a multi-disciplinary open access archive for the deposit and dissemination of scientific research documents, whether they are published or not. The documents may come from teaching and research institutions in France or abroad, or from public or private research centers.

L'archive ouverte pluridisciplinaire **HAL**, est destinée au dépôt et à la diffusion de documents scientifiques de niveau recherche, publiés ou non, émanant des établissements d'enseignement et de recherche français ou étrangers, des laboratoires publics ou privés.

## Accepted Manuscript

An experimental study of failure initiation and propagation in 2D woven composites under compression

N.V. De Carvalho, S.T. Pinho, P. Robinson

PII: S0266-3538(11)00152-7  
DOI: [10.1016/j.compscitech.2011.04.019](https://doi.org/10.1016/j.compscitech.2011.04.019)  
Reference: CSTE 4980

To appear in: *Composites Science and Technology*

Received Date: 29 December 2010  
Revised Date: 30 March 2011  
Accepted Date: 28 April 2011

Please cite this article as: De Carvalho, N.V., Pinho, S.T., Robinson, P., An experimental study of failure initiation and propagation in 2D woven composites under compression, *Composites Science and Technology* (2011), doi: [10.1016/j.compscitech.2011.04.019](https://doi.org/10.1016/j.compscitech.2011.04.019)

This is a PDF file of an unedited manuscript that has been accepted for publication. As a service to our customers we are providing this early version of the manuscript. The manuscript will undergo copyediting, typesetting, and review of the resulting proof before it is published in its final form. Please note that during the production process errors may be discovered which could affect the content, and all legal disclaimers that apply to the journal pertain.



# An experimental study of failure initiation and propagation in 2D woven composites under compression

N. V. De Carvalho<sup>\*,a</sup>, S.T. Pinho<sup>a</sup>, P. Robinson<sup>a</sup>

<sup>a</sup>*Department of Aeronautics, Imperial College London, Prince Consort Road, South Kensington, London SW7 2AZ. UK.*

---

## Abstract

Experimental research was conducted to investigate the compressive failure of orthogonal 2D woven composites. Damage initiation and the effect of weave architecture were studied using a Four Point Bending (FPB) test setup. Scanning Electron Microscope (SEM) and Digital Imaging (DI) observations show the individual failure of the load-aligned tows, which behave as structural elements at the internal reinforcement level. Weave architecture and internal geometry are seen to affect location and morphology of the damage initiation.

Damage propagation and the effect of stacking were studied using a reduced Compact Compression (rCC) test setup. Optical micrographs show that stacking configuration can have a significant effect on the damage morphology. Additionally, results also suggest the effect of stacking is a function of the weave architecture and internal geometry.

*Key words:* A.Textile composites, B.Fracture, C.Damage mechanics, D.Fractography, D.Scanning electron microscopy (SEM)

---

## 1. Introduction

The ability to accurately predict and model the mechanical and structural response of composite materials is essential to optimise their use, to reduce the number of experiments needed to validate new designs/materials, and to support the development of improved materials. In the last decades, the response of unidirectional (UD) composites under different loadings and their failure mechanisms have

---

\*Corresponding author  
Email address: [nvieirad@imperial.ac.uk](mailto:nvieirad@imperial.ac.uk) (N. V. De Carvalho)

been studied by numerous authors. Although good agreement can be found concerning the description of the failure mechanisms, their full understanding and accurate modelling are not yet accomplished [1]. The variability of woven composites, inherent to their reinforcement architecture, promotes the interaction between different micro-mechanical failure mechanisms, increasing the difficulty when studying their failure. Therefore, insightful experimental research is fundamental to support the development of tools effectively capable of predicting and modelling failure [2].

The detailed study of the compressive failure mechanisms in woven composites is hindered by: (i) the typically sudden nature of compressive failure, and (ii) the need to understand the effect of the reinforcement geometry on the failure process. Therefore, it is not surprising that most of the literature highlights the final failure morphology rather than the nature and development of the failure process. From the available literature, it is possible to conclude that kink-band formation, as well as intra-ply and inter-ply delamination, are the main compressive failure mechanisms of orthogonal 2D woven composites [3–5]. Final failure results from the interaction of these mechanisms which in turn are determined by variables such as reinforcement architecture, loading rate, confinement and mechanical properties of the resin. The latter have a decisive influence on the predominance of the different mechanisms. In general, brittle resins favour delamination while tougher resins tend to induce kink band formation and overall shear failure [5, 6]. In addition, high loading rate and confinement induces kink band dominated failure [7, 8]. Although the main compressive failure mechanisms have been identified, failure initiation has not been subject to widespread and detailed study. An exception is the work from Mirzadeh and Reifsnider [9] on the damage initiation and failure in compression of a 8H satin carbon-polyimide material system. Compression tests were stopped before final failure, and the edges of the specimens observed. The test procedure was successful in identifying kinking of the load-aligned tows as the predominant damage mechanism controlling the failure process. The authors also tested notched specimens. In the latter, failure initiated at the surface of the specimens at the notch and also at the crimp regions of the tows close to the notch. These findings highlight the importance of the reinforcement architecture in the failure process. However, the effect of the reinforcement architecture was not investigated.

Since woven plies are not flat, when manufacturing a laminate, coincident valleys and peaks of



adjacent layers will nest, resulting in a decrease in resin-rich areas. The relative positioning of adjacent layers with the same orientation, hereafter referred to as stacking, determines the number of coincident valleys and peaks between adjacent layers and, therefore, affects strongly the degree of nesting. Very few studies have discussed the effect of stacking (and resultant nesting) on the failure of woven composites [9–13]. Breiling and Adams [10], studying the compressive failure of a 5H satin carbon-epoxy, concluded that varying the stacking configuration (i.e. the relative position of peaks and valleys of adjacent mats with the same orientation), could lead to a reduction of up to 32% on the ultimate strength. However, a relation between the failure mechanisms and the different stacking configurations was not established. Understanding the effect of stacking and consequent nesting in the failure process is essential to develop meso-scale models (analytical or numerical) that capture the physics of the failure process.

This work presents a detailed analysis of the compressive failure process of orthogonal 2D woven composites. The aim is to gather insight on the failure mechanisms and investigate the effect of the reinforcement architecture on the failure process. Section 2 provides details on the material systems used,  $2 \times 2$  Twill and 5H Satin, and their manufacture process. Additionally, it also describes the two test setups used: FPB and rCC. The FPB test setup is used to explicitly study the effect of the weave architecture on the failure initiation sequence and morphology under compression. The rCC test setup is used to characterise the compressive damage propagation in general, and in particular the effect of stacking on the failure mechanisms. In Section 3.1, the results obtained with the FPB test setup are presented. SEM and DI images of failed specimens with different weave architectures are compared. Section 3.2 shows the results obtained with the rCC test setup. Optical micrographs are presented comparing the damage morphology obtained for the different weaves and stacking configurations. Section 4 provides a discussion of the results obtained and Section 5 presents the main conclusions from the work developed.

## 2. Experiments

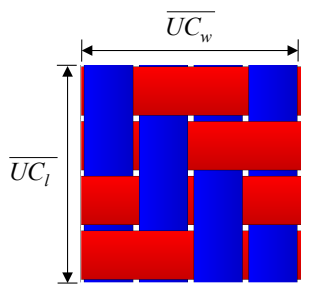
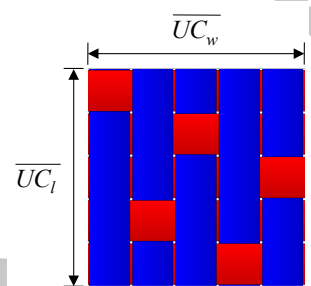
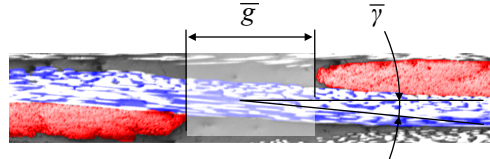
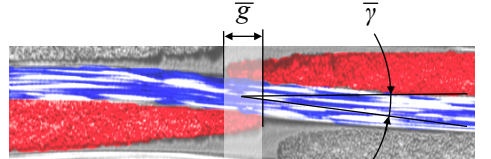
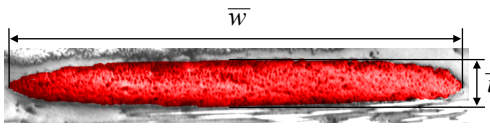
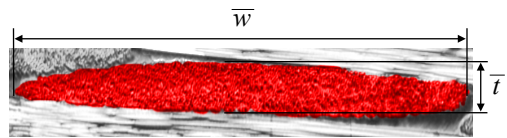
Two different experimental setups were used: Four Point Bending (FPB) and reduced Compact Compression (rCC) [14]. The FPB setup was used to study the damage initiation mechanisms and

their relation with the weave architecture/geometry. The rCC setup was used to study and characterise the damage propagation mechanisms and investigate how are they affected by stacking and weave architecture.

### *2.1. Material Systems*

Two balanced 2D woven carbon-epoxy prepregs with different weave architectures were used. The differences between the weave architectures of the two materials are highlighted in Table 1, where their idealized Unit Cells are shown. The areal density of the two prepregs was obtained from the manufacturer and is provided in Table 1. In the present work, the geometry of the reinforcement constituents after curing, such as the shape of the cross-section of the tows and the distance between tows, is referred to as “weave geometry”. The statistical characterisation of the weave geometry of the two materials can also be found in Table 1. Thirty measurements of each dimension were made on micrographs obtained from samples of cured material, illustrated in Table 1. Concerning the weave geometry, the main difference between the two weaves is the size of the average gap ( $\bar{g}$ ) between adjacent tows. The latter is larger in the twill than in the satin. Indeed, adjacent tows in the satin weave are partially superposed (negative average gap). The crimp angle ( $\bar{\gamma}$ ) is defined as the angle of the load aligned tows relative to the loading direction measured at the centre of the crimp region. Table 1 shows that the crimp angle ( $\bar{\gamma}$ ) is larger in the satin than in the twill. Width ( $\bar{w}$ ) and thickness ( $\bar{t}$ ) of the cross section of the tows are similar in both weaves, with the satin tows being slightly thicker on average.

Table 1: Characterisation of the two materials used. The areal density of the prepregs was obtained from the manufacturer. Remaining measurements (30 for each dimension) were performed on micrographs obtained from samples of cured material.  $\overline{UC}_l$  and  $\overline{UC}_w$  are, respectively, the average length and width of the unit cells.  $\bar{g}$  is the average length of the gap between adjacent tows;  $\bar{\gamma}$  is the average angle of the load aligned tow relative to the loading direction, measured at the centre of the crimp region.  $\bar{w}$  and  $\bar{t}$  are, respectively, the average width and thickness of a cross-section of a tow.

$2 \times 2$ Twill: T300/920CX-3K	5H Satin: M56/AS4-3K
Areal density = 368 g/m <sup>2</sup> , $V_f = 45\%$	Areal density = 444 g/m <sup>2</sup> , $V_f = 53\%$
Weave architecture - Unit Cell	
	
$\overline{UC}_l = \overline{UC}_w = 8.36 \pm 0.61$ mm	$\overline{UC}_l = \overline{UC}_w = 7.93 \pm 0.95$ mm
Crimp Region	
	
$\bar{g} = 0.51 \pm 0.07$ mm, $\bar{\gamma} = 6.4^\circ \pm 2.3^\circ$	$\bar{g} = -0.08 \pm 0.06$ mm, $\bar{\gamma} = 8.5^\circ \pm 2.1^\circ$
Tow cross section	
	
$\bar{w} = 1.58 \pm 0.08$ mm, $\bar{t} = 0.15 \pm 0.01$ mm	$\bar{w} = 1.58 \pm 0.13$ mm, $\bar{t} = 0.17 \pm 0.06$ mm

## 2.2. Manufacture and Testing

### 2.2.1. Four Point Bending (FPB)

As mentioned previously, the detailed study of the compressive failure initiation of 2D woven carbon-epoxy composites is hindered by the sudden nature of compressive failure, and the need to understand the effect of the weave architecture and geometry on the failure process. In the present

study, these difficulties are tackled using a tailored specimen design (lay-up and dimensions) combined with the FPB setup.

### *Manufacture*

From each material system (Table 1), one plate consisting of 16 plies was laid-up using standard methods for prepreps and cured in an autoclave following the instructions from the manufacturer. Outer and inner plies were oriented at  $0^\circ$  and  $45^\circ$ , respectively,  $[0^\circ, 45^\circ]_S$ . Having a higher strain to failure, the  $45^\circ$  layers were included to help prevent the sudden failure of the specimen. In the satin specimens, one of the  $0^\circ$  outer layers was warp-dominated while the other was weft-dominated. A layer of satin is considered to be warp-dominated if its surface has more warps than wefts and vice-versa. This enabled to study the effect of the surface dominance by choosing which side of the specimen (warp-dominated/weft-dominated) was under compression. Both plates were C-scanned after manufacturing to access their quality. Ten specimens were cut from each plate. The nominal dimensions of the specimens were  $L_{FPB} = 155$  mm in length, width  $w_{FPB} \approx 40$  mm and thickness  $t_{FPB} = 4$  mm, Fig. 1. All dimensions follow the ASTM specifications with exception of the width [15]. The latter was chosen to be approximately equal to the length of 5 UCs, see Fig. 1, to help ensuring the unit cells in the centre of the specimen were not affected by edge effects. It is important to highlight that the specimens are unnotched to enable the study of the effect of the weave architecture on the damage initiation.

### *Test setup*

The FPB setup used is illustrated in Fig. 1. In the FPB setup, the specimen is loaded such that its top/bottom surfaces are under compressive/tensile loading. This setup, combined with the specimen design previously described, enables the observation of damage initiation in the  $0^\circ$  outer ply loaded in compression, prior to the catastrophic failure of the specimen. In the present study, only the damage occurrences in the central area of the outer layer loaded in compression are considered. The central area is defined as a rectangle having its edges at a distance of 1 UC from the specimen edges and the upper loading pins, Fig. 1. This definition guarantees the standardization of the observations and eliminates from the analysis possible damage occurrences caused by the stress concentrations at the pins and edge effects. All pins have radius  $r = 3$  mm. The distance between the lower pins is

$l = 128$  mm, and between the upper pins  $l/2$ . Rubber bands were placed between the loading pins and the specimens to prevent localised damage and early failure due to stress concentrations.

Acoustic Emission (AE) was used as an auxiliary tool to detect and locate damage events as the test progressed. An AE suite manufactured by Physical Acoustic Corporation [16] was used. Two broadband sensors, with a frequency range [100 kHz, 1000 kHz], were mounted on the specimen surface close to the upper pins, as shown in Fig. 1. The sensors were secured with elastic bands and silicon grease was used as a coupling agent.

The testing procedure was as follows: (i) each specimen was placed on the rig, (ii) the AE sensors were mounted and calibrated, (iii) loading was applied, (iv) the tests were stopped at two stages: (a) immediately after the first failure occurrence was detected (through visual inspection and AE monitoring), and (b) after several occurrences were detected, in order to be able to study the first stages of the failure initiation, (v) the specimens were removed from the rig and digital images of the compression side were collected, and (vi) damage details were further investigated using SEM.

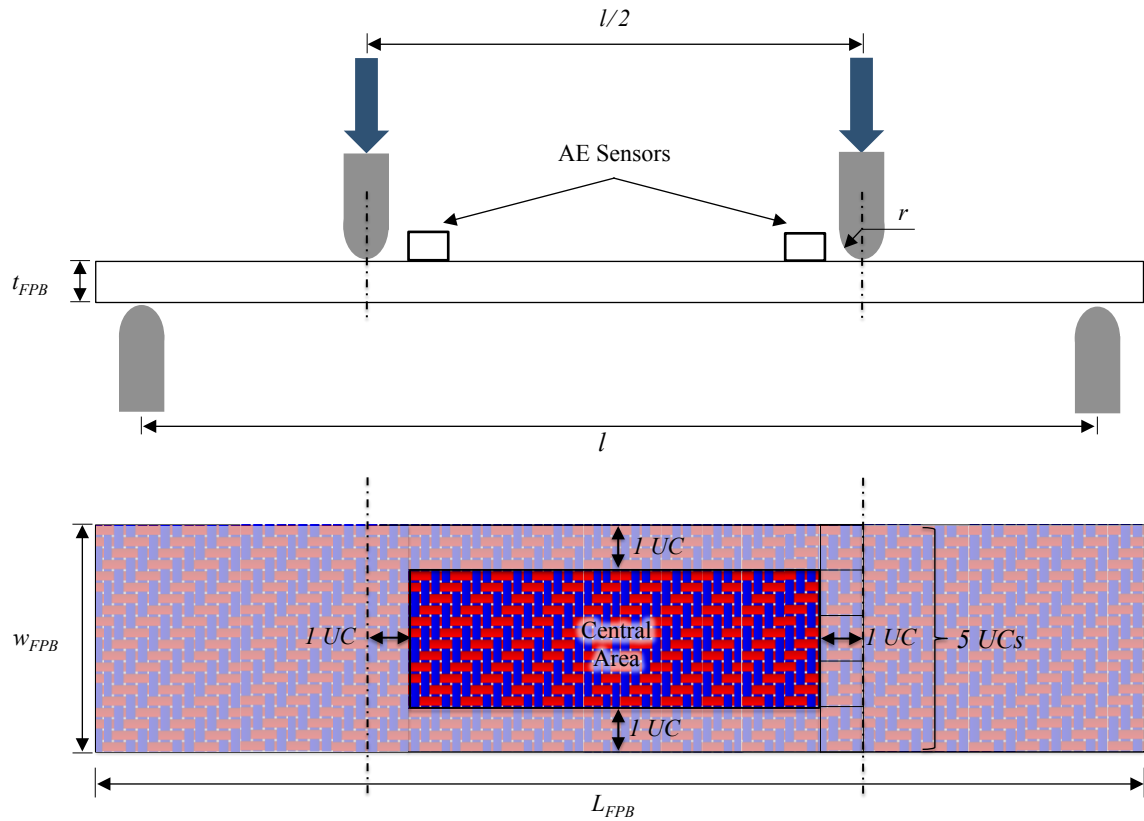


Figure 1: Four Point Bending test setup and specimen dimensions. Only damage occurrences in the central area of the  $0^\circ$  outer ply loaded in compression are considered. The central area is defined as a rectangle having its edges at a distance of 1 UC from the specimen edges and the upper loading pins.

### 2.2.2. reduced Compact Compression (rCC)

Using a notched specimen, the rCC setup [14] enables compressive damage to propagate in a non-catastrophic fashion. Upon loading, damage initiates at the notch tip and propagates stably towards the back of the specimen, Fig. 2. Using the rCC setup instead of the traditional Compact Compression (CC) [17] enabled the use of specimens with smaller dimensions. Therefore, smaller plates could be produced which provided an improved control over the stacking in the manufacturing of the ordered-stacked plates. In the present study the rCC setup is used to: (i) identify and observe the compressive

damage mechanisms, (ii) study the effect of stacking on the damage morphology and (iii) investigate if the effect of stacking on the damage morphology is affected by the weave architecture and geometry.

#### *Manufacture*

The two materials identified in Table 1 were also used. For each material system, two plates consisting of 12 plies each were manufactured:

1. Ordered-stacked, Fig 3a: All plies were laid-up with the same orientation,  $0^\circ$  warp aligned,  $[0_{12}^\circ]$ . When laying-up, the UCs of each ply were carefully positioned on top of the corresponding UCs of the previously laid plies, without any shifts. To facilitate this, the cutting of the prepreg plies was made tow-number-wise and not dimension-wise. Additionally, pins were used to fix the plies at defined positions.
2. Random-stacked, Fig. 3b: All plies were laid-up with the same orientation,  $0^\circ$  warp aligned,  $[0_{12}^\circ]$ . When laying-up, the relative positions of the adjacent UCs were not considered, leading to random shifts (but not rotations) between layers.

After lay-up, the plates were cured in an autoclave following the instructions from the manufacturer. After manufacturing, the plates were C-scanned to assess their quality. Fourteen rCC specimens were manufactured in total; their nominal dimensions were  $t = 3$  mm,  $l = w = 20$  mm and the notch length was  $n = 14$  mm, Fig. 2b. The notch tip was made using a band saw (radius  $\sim 2$  mm).

#### *Test setup*

The rCC specimens were loaded in compression using the rig shown in Fig. 2a. The rCC setup enables the stable initiation and propagation of a crack that initiates at the notch tip. The testing procedure was as follows: (i) each specimen was placed in the rig and compressive loading was applied, (ii) the test was stopped once a crack propagating from the notch was visually observed, (iii) the specimen was removed from the rig and potted in resin, (iv) the potted specimens were ground and polished as indicated by section TT in Fig. 2b, (v) using an optical microscope the through-thickness sections (TT) were inspected for damage, and (vi) steps iv) and v) were repeated until the crack tip was found as a result of the additional grinding.

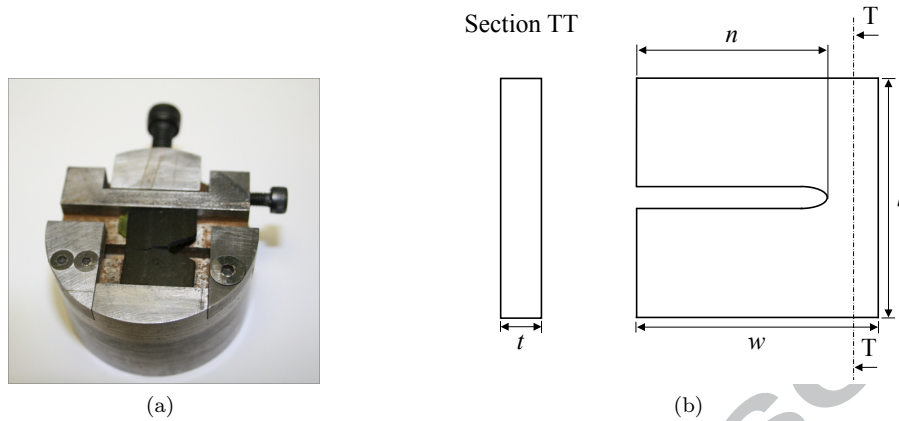


Figure 2: a) rCC rig [14]; and b) specimen dimensions.

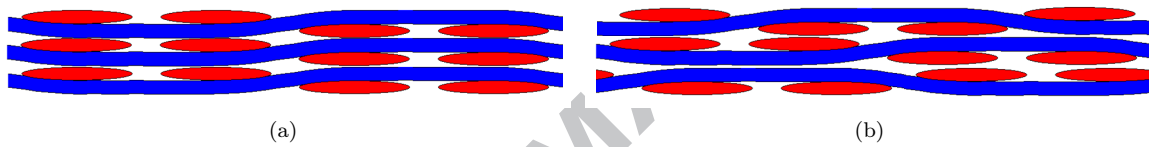


Figure 3: a) ordered-stacking; b) random-stacking

### 3. Results

#### 3.1. FPB: damage initiation & reinforcement architecture

In the twill specimens, the first type of damage occurrence registered was the failure of a tow at the Crimp Region (CR), suggesting the relevance of this region in the compressive failure of twill composites, Fig. 4. As mentioned previously, some specimens were stopped at a later stage, when more than one damage occurrence in the central area of the compressive surface could be observed, Fig. 5a. In the twill case, these consisted of tows failed at different regions (the classification used in Fig. 5 will be detailed later).

In the satin specimens failure initiation was more abrupt than in the twill specimens, with multiple failure sites initiating almost simultaneously, Figs. 5b and 5c. In the warp-dominated satin specimens, the damage morphology was similar to the twill specimens, consisting essentially of tows that failed discretely at different regions. However, comparing the compressive surface of twill and satin specimens,



Fig. 5, it is evident that the damage morphology of the weft-dominated satin specimens is different from the remaining two (twill and warp-dominated satin). Besides discretely failed tows, weft-dominated satin specimens also show a crack spanning several crimp regions along the same weft tow, Fig. 5c.

In the testing of both satin and twill specimens, after several tows failed in the central area of the compressive side of the specimens, final failure occurred rapidly through the development of a crack spanning several failed tows. The latter occurred either below one of the loading pins or in the central area of the specimen.

To facilitate the analysis, tow failures are classified according to the area of the tow where the failure occurs: Crimp Region (CR), Middle of the Upper Float (MUF), and Other Regions (OR) if the tow fails anywhere other than CR or MUF, Fig. 5. Moreover, it is also possible to observe that some adjacent tows failed in neighbouring regions; e.g. tows failed at MUF immediately adjacent to tows failed at CR. This type of occurrence is named CR-MUF. A particular feature of the warp-dominated satin specimens is the occurrence of tows failed at OR adjacent to tows failed at CR. This type of occurrence is designated OR-CR, Fig. 5.

Although most tows fail at CR, tows failed at other regions can also be identified. To give quantitative support to the observations made, a representative number of failed tows and respective locations was counted. Figure 6 compares the percentage of failed tows in each area in twill and satin warp-dominated specimens. In both cases, and as qualitatively appreciated before, most tows fail at CR. In the twill specimens tows fail preferentially at MUF rather than at OR. In the satin case, the difference between the percentage of tows failed at OR and MUF is not significant. The latter is due to an increase in OR-CR occurrences.

Having identified CR as critical in the compressive failure of all specimens, Fig. 7 provides a closer detail of tows failed at this region. All tows represented in Fig. 7 failed in an isolated fashion, i.e. they are not part of a crack developing along the specimen surface and they are not adjacent to tows failed in neighbouring regions. Their limits can be clearly identified by cracks following the interface between tows and pure matrix regions, suggesting significant out-of-plane movement. Comparing the three cases, it is possible to see that, in twill and weft-dominated satin specimens, tows fail at the centre of the CR, while in warp-dominated specimens, tows fail at a non-negligible distance  $d \neq 0$  from

the centre of the CR.

As mentioned previously, in twill and warp-dominated satin specimens, some adjacent tows failed in neighbouring regions, namely CR-MUF and OR-CR, Fig. 5. Comparing the morphology of CR-MUF occurrences in the twill and in the satin warp-dominated specimens, Figs. 8a and 8b, it is possible to see that the failure locus of neighbouring tows failed at MUF and CR are adjacent to each other in the twill case, while in the satin case they are not. The latter is due to the fact that, in warp-dominated satin specimens, CR failure occurs at a small distance  $d \neq 0$  from the CR centre, as mentioned previously, Fig. 8b. In CR-MUF occurrences, tows fail in an isolated fashion with their limits identifiable by cracks following the interface between tows and pure matrix regions. In warp-dominated satin specimens, besides CR-MUF, also OR-CR occurrences were registered, Fig. 8c. In the latter, and contrarily to what was observed in the CR-MUF occurrences, damage was seen to propagate from one tow to the other in a seemingly continuous fashion.

Finally, Fig.9 examines in more detail the damage morphology of a failed tow. Analysing Fig. 9 it is possible to identify a kink band in the central part of the tow, suggesting the tow failed by kinking. In all tows analysed at the SEM (both twill and satin), kinking was identified as the damage mechanism responsible for their failure.

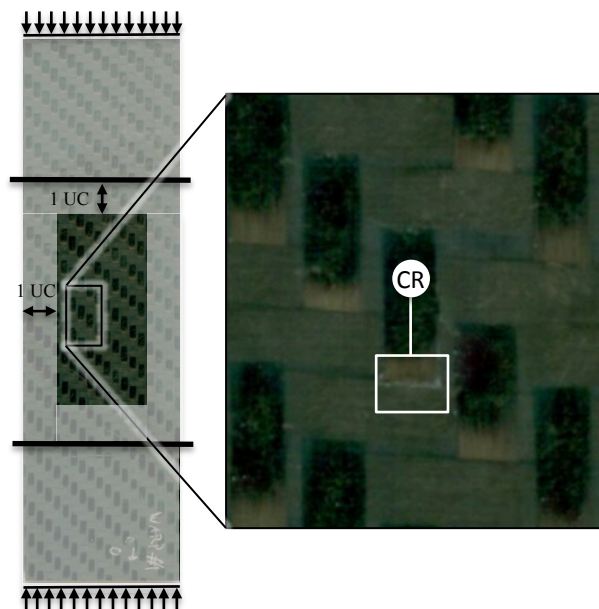
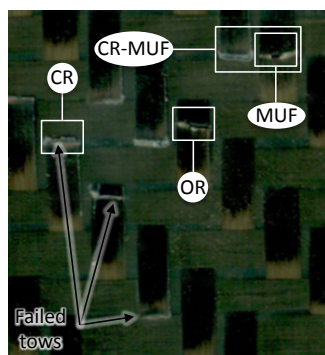
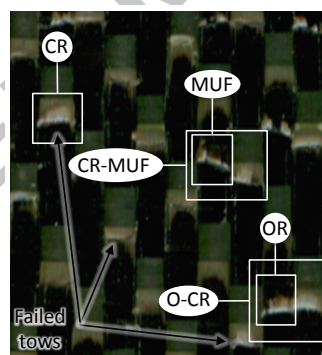


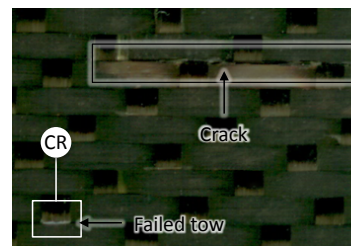
Figure 4: Compressive side of a  $2 \times 2$  twill FPB specimen. Test was stopped after the first damage in the central region of the compressive side was detected - failed tow at the Crimp Region (CR).



(a)  $2 \times 2$  twill



(b) 5H satin: warp-dominated surface



(c) 5H satin: weft-dominated surface

Figure 5: Comparison between the damage morphology registered in the different specimens tested. The test was stopped after several damage occurrences were detected and before the failure of the specimen. The failed tows are classified according to the region of the tow where the failure occurs: Crimp Region (CR); Middle of the Upper Float (MUF) and Other Regions (OR). Additionally, the designations CR-MUF and CR-OR refer to neighbouring regions where adjacent tows fail at CR and MUF or OR.

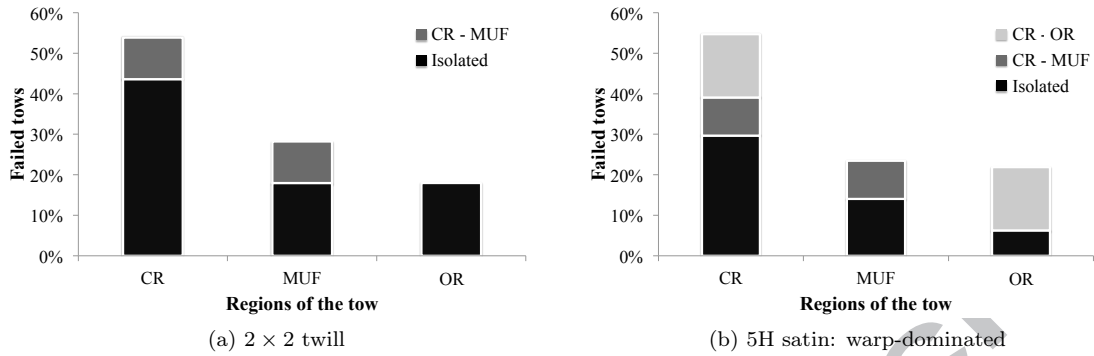


Figure 6: Percentage of failed tows at the different regions: Crimp Region (CR), Middle of the Upper Float (MUF) and Other Regions (OR). CR-MUF and CR-OR refer to neighbouring regions where adjacent tows fail at the CR and MUF or OR, respectively. Data was collected from 6 twill specimens (38 failed tows), and 3 warp-dominated satin specimens (64 failed tows).

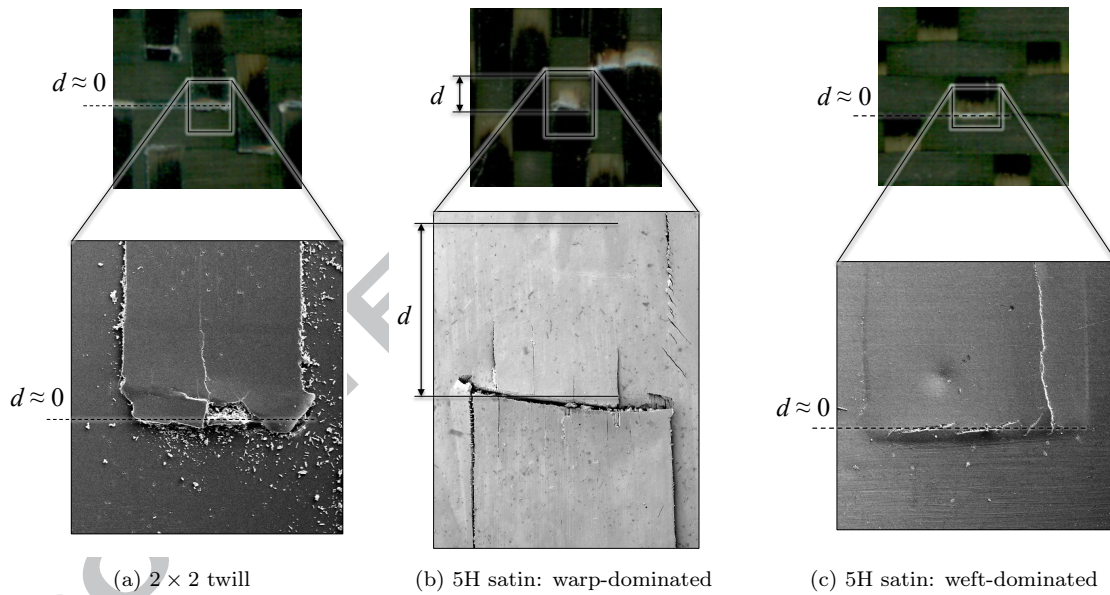
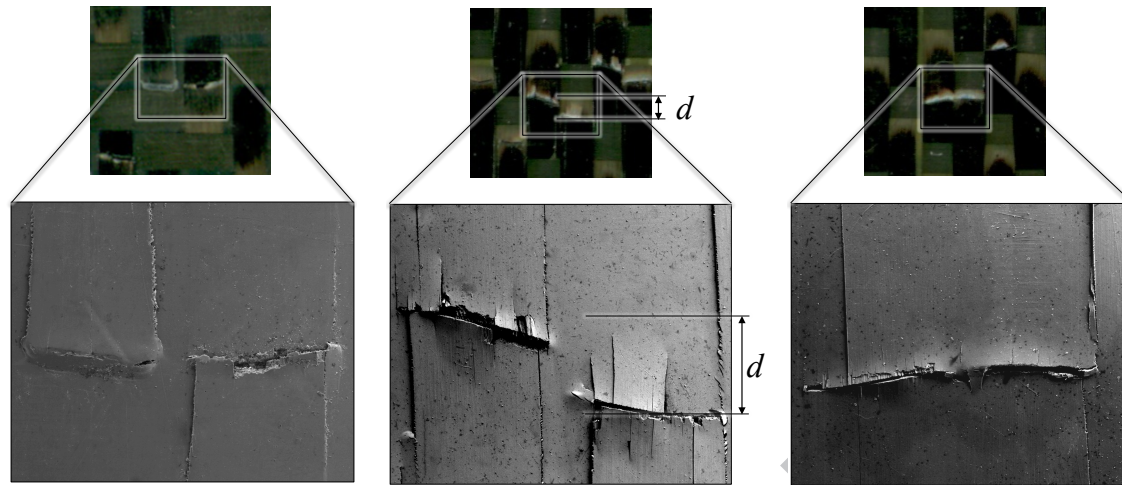


Figure 7: Location of the failure relative to the centre of the CR. In (a) and (c) the load-aligned tows fail close to the centre of the CR,  $d \approx 0$ , while in (b) they fail at a non-negligible distance  $d$ .

(a)  $2 \times 2$  twill: CR-MUF

(b) 5H satin: CR-MUF

(c) 5H satin: CR-OR

Figure 8: Adjacent tows failed at CR-MUF and CR-OR observed in twill and satin warp-dominated specimens. In twill specimens the failure locus of neighbouring tows failed at CR and MUF are adjacent, while in the warp-dominated satin specimens they have a non-negligible distance  $d$  between them. In CR-MUF occurrences tows fail in an isolated fashion, while in CR-OR occurrences damage propagates from one tow to the other in a seemingly continuous fashion.

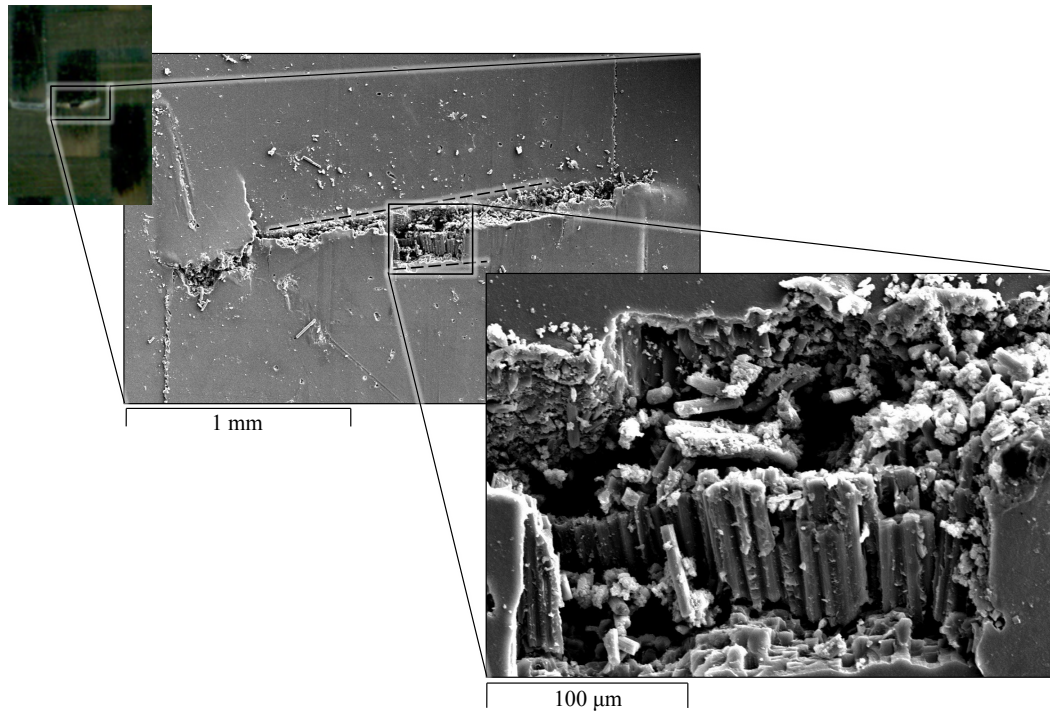


Figure 9: Detail of a tow failed by kinking in a twill specimen.

### 3.2. *rCC*: damage propagation and stacking

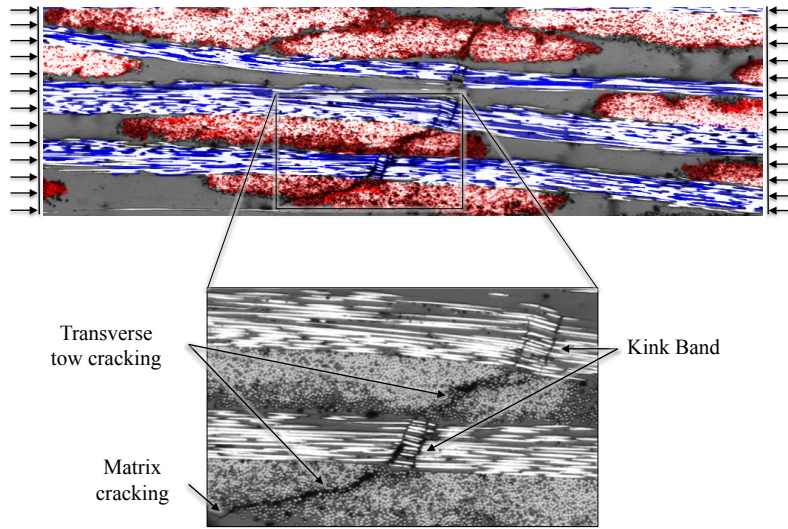
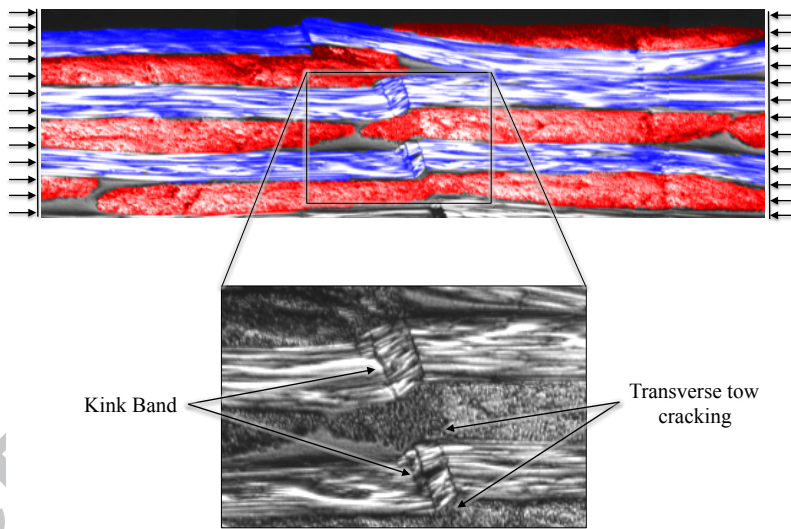
In random-stacked *rCC* specimens, the damage propagated by kinking of the load-aligned tows and cracking of the transverse tows and matrix. Both satin and twill specimens show a similar morphology, Fig. 10.

Figure 11 compares the damage morphology observed in two representative ordered-stacked specimens, twill and satin. The ordered-stacking can be accessed by comparing the position of the centre of the CR in adjacent layers, highlighted in Fig. 11. Analysing Fig. 11a, it is clear that the ordered-stacked twill specimens show a different damage morphology from the one observed in the random-stacked specimens, Fig. 10a. The load-aligned tows show pronounced bending, associated with delamination between tows and matrix. Within the tows, splitting between fibres and several fibre breaks can also be observed. This type of damage occurred systematically at the crimp regions. In the satin specimens the differences between the damage morphology of ordered and random-stacked

specimens are less obvious, Figs 11b and 10b, respectively. In both cases, damage propagates by kink band formation, matrix and transverse tow cracking. Nevertheless, the ordered-stacked specimens show, in general, more delamination between transverse and load aligned tows, Fig. 11b. Contrarily to the twill, no visible damage concentration can be found at the crimp regions on the satin ordered-stacked specimens and the significant bending of the tows prior to the failure was less obvious.

ACCEPTED MANUSCRIPT

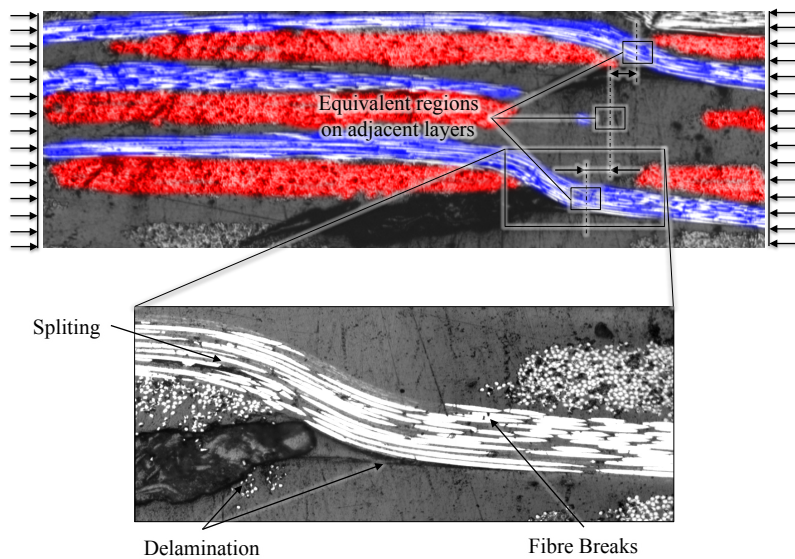
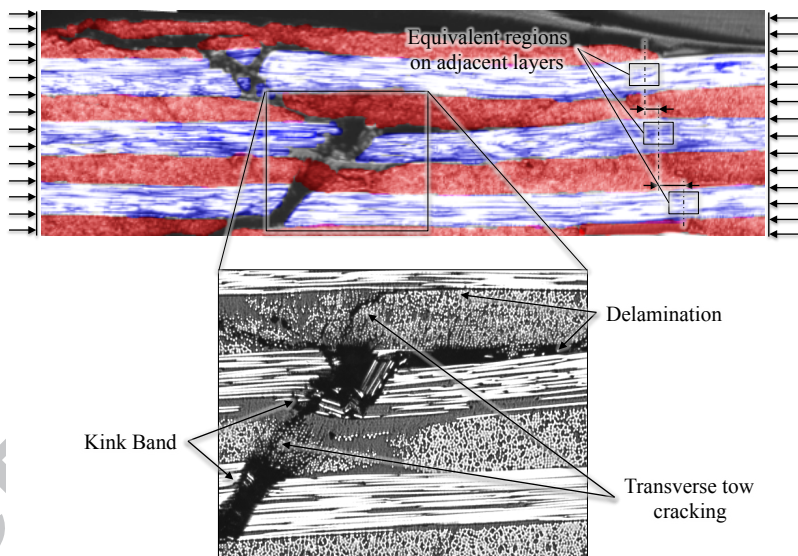


(a)  $2 \times 2$  twill: random-stacked.

(b) 5H satin: random-stacked.

Figure 10: Comparison between the damage morphology of  $2 \times 2$  twill and 5H satin random-stacked specimens. In both specimens, the damage propagation mechanisms observed were kinking of the load aligned tows and cracking of the transverse tows and matrix.



(a)  $2 \times 2$  twill: ordered-stacked.

(b) 5H satin: ordered-stacked.

Figure 11: Comparison between the damage morphology of  $2 \times 2$  twill and 5H satin ordered-stacked specimens. The ordered-stacking is highlighted by comparing the position of the centre of the CR in adjacent layers. The twill specimen shows pronounced bending of the load-aligned tow associated with delaminations between the latter and matrix. Fibre breaks and splits between fibres within the tow are also observed. The satin specimen shows delamination between load-aligned and transverse tows, cracking of the transverse tows and kinking of the load-aligned tows.

## 4. Discussion

### 4.1. FPB: damage initiation & reinforcement architecture

#### 4.1.1. Overview

From the observations presented, it is apparent that: (i) tows behave as structural elements at the reinforcement level, (ii) damage morphology is affected by the weave architecture and geometry, (iii) tows tend to fail at the crimp region, and (iv) kinking is the main failure mechanism responsible for the failure of the load-aligned tows.

#### 4.1.2. Structural role of the tows

The structure role of the tows can be inferred from the discrete nature of the damage observed - tows fail individually with significant out-of-plane movement. Moreover, even in areas where adjacent tows fail in neighbouring regions, tows were seen to fail individually (CR-MUF). The latter suggests that load transfer between the first tow failing and the adjacent tow was the mechanism responsible for the local damage propagation.

#### 4.1.3. Effect of the weave architecture

The damage morphology varied with weave architecture. The differences in damage morphology between weft-dominated satin specimens and twill/warp-dominated satin are the most obvious. However, a detailed analysis shows that damage morphology is also different between twill and warp-dominated satin specimens, e.g. location of the failure at the CR.

#### 4.1.4. Crimp region

In all specimens tested, the crimp region was seen to be critical. In weft-dominated satin specimens, a central crack developed along a weft tows connecting CRs. Additionally, the isolated failures registered occurred at CR. In twill and warp-dominated satin specimens, most tows failed at CR. Moreover, a large percentage of tows failed at MUF and OR were adjacent to tows failed at CR. The latter suggests tows failed first at the CR and then, via load transfer, caused the failure of adjacent tows in a neighbouring region. The relevance of the CR in the compressive failure of woven composites was partially expected. In this region, fibres within the tow are significantly misaligned with respect to the loading direction. However, local misalignment alone does not explain all the details of the damage morphology observed. Having into account the misalignment is maximum at the centre of the

crimp region, failure would be expected to occur at this location. However, in warp-dominated satin specimens, tows failed systematically at a small distance  $d$  from the centre of the CR. This observation reinforces the importance of explicitly considering weave architecture and geometry when analysing the compressive response of 2D woven composites.

#### 4.1.5. Tow failure - fibre kinking

Observations showed the load-aligned tows failed by kinking. At the microscale, kink band formation in woven and UD composites is expected to occur in a similar fashion: opening of micro-cracks/plasticity of the matrix ultimately leading to kinking [14, 18]. However, while in UD composites the initiation of kink band formation is essentially related to local misalignment/defects, in woven composites it is additionally affected by the local response of the reinforcement and therefore by the weave architecture.

### 4.2. rCC: damage propagation and stacking

#### 4.2.1. Overview

From the observations presented, it is possible to infer that: (i) kink band formation, matrix cracking and transverse tow cracking are the predominant damage propagation mechanisms in compression (ii) stacking, and therefore the support provided by adjacent layers, affects the damage mechanisms (iii) the effect of stacking is weave dependent.

#### 4.2.2. Damage mechanisms

The load-aligned tows were seen to fail by kink band formation. Regions of cracked matrix and/or transverse tows, connected adjacent tows failed by kink band formation, forming a damage band.

#### 4.2.3. Effect of stacking on the damage morphology

Stacking was seen to affect the damage morphology, particularly in the twill specimens. This observation highlights the importance of the support provided by the adjacent layers upon loading. Moreover, it is also consistent with the observations made in Section 3.1, namely the behaviour of tows as structural elements at the reinforcement level. Figure 12a shows an idealised load-aligned tow, assumed to behave as a load carrying beam-column embedded in an elastic foundation (matrix). The arrows indicate its anticipated deflection direction due to the applied load. Figure 12b represents the

same tow, together with two adjacent tows, representing an ordered-stacked laminate. All tows are expected to behave as load carrying beam-columns. It can be easily observed that the anticipated displacement of the tows are all compatible and in-phase. Figure 12c shows the same tow but now in a random-stacked laminate. In contrast to the case observed in Fig. 12b, not all the anticipated displacements in Fig. 12c are compatible. Indeed, some regions of the adjacent tows will act to reduce the deflection of the embedded load-aligned tow, providing increased support. Moreover, in the random-stacked case, the adjacent transverse tows (dashed) might replace the matrix near the crimp regions due to nesting, while in the ordered-stacked this area is surrounded by pure matrix. Additionally, it is important to highlight that ordered-stacking is one of the possible arrangements present in a random-stacked laminate. The presence of regions of ordered-stacked layers in a woven laminate will contribute to the variability of the damage mechanisms in 2D woven composites and consequently of their measured properties.

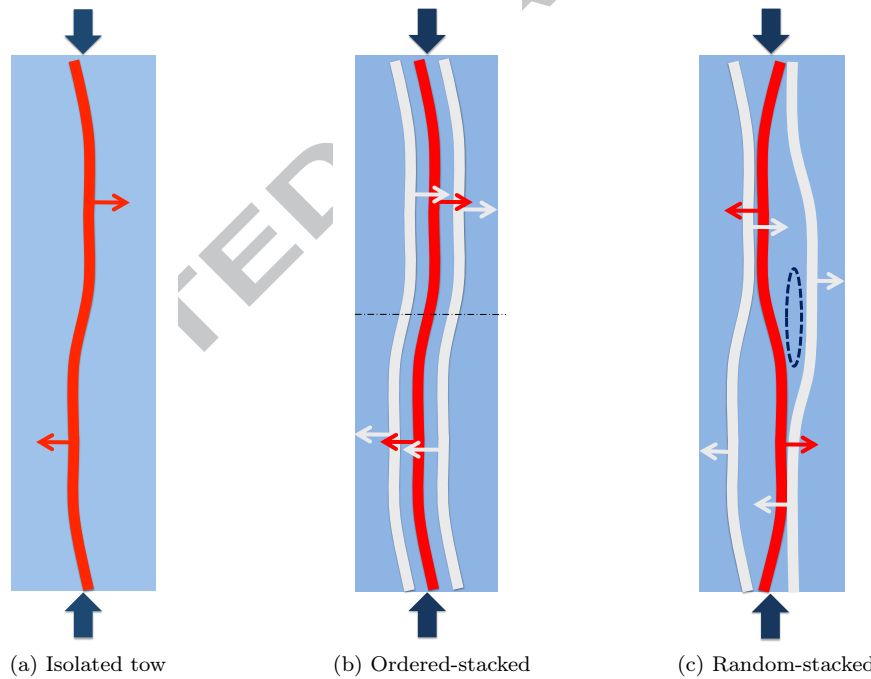


Figure 12: Effect of stacking on the interaction between tows during compression

#### 4.2.4. Weave dependence of the effect of stacking on the damage morphology

The effect stacking was more pronounced in the twill than in the satin specimens. This suggests that depending on the weave architecture and geometry, this effect can be more or less significant. Two main factors might contribute to the difference registered. The first has to do with the global response of the internal reinforcement. Upon compressive loading, the out-of-plane deflection of the load-aligned tows will vary as a function of tows' shape and weave pattern. Therefore, the effect of the variation in local support will be higher for weaves that, due to their weave pattern and geometry, have a larger out-of-plane deflection upon loading. Another seemingly relevant factor, with a more localized effect, is the tightness of the weave. Comparing the crimp regions of both weaves, Table 1, it is possible to see that the crimp region of the satin weave is surrounded by transverse tows, providing additional support, while for the twill weave the central portion of the crimp region is surrounded by pure matrix.

## 5. Conclusions

Using a FPB test setup and a tailored specimen design, damage initiation in compression was investigated for two different 2D woven composites. From the results obtained, it is possible to conclude that: (i) tows behave as structural elements at the reinforcement level, (ii) damage morphology is affected by the weave architecture and geometry, (iii) tows tend to fail at the crimp region and (iv) kinking is the predominant failure mechanism responsible for the failure of the load-aligned tows.

Using a rCC test setup, damage propagation in compression for two different 2D woven composites and the effect of different stacking configurations was investigated. It can be concluded that: (i) kink band formation, matrix cracking and transverse tow cracking are the predominant damage propagation mechanisms in compression (ii) stacking, and therefore the support provided by adjacent layers, affects the damage mechanisms (iii) the effect of stacking is weave dependent.

Failure criteria developed for UD are often applied to predict failure of 2D woven composites. However, the present study indicates that, to capture the physics of the compressive failure of 2D woven composites, the weave architecture needs to be considered, both at lamina and laminate level.

UC meso-scale finite element models are increasingly used for predicting the failure strength of

2D woven composites. In this approach, the details of the weave architecture are included. However, these models are normally single ply models, not accounting for the effect of the support given by the adjacent layers. The current study suggests the effect of the support (although weave dependent) is not negligible.

## References

- [1] P.D. Soden M.J. Hinton, A.S. Kaddour, editor. *Failure Criteria in Fibre Reinforced Polymer Composites: The World Wide Failure Exercise*. Elsevier Science, 2004.
- [2] S.V. Lomov, D.S. Ivanov, T.C. Truong, I. Verpoest, F. Baudry, K.V. Bosche, and H. Xie. Experimental methodology of study of damage initiation and development in textile composites in uniaxial tensile test. *Composites Science and Technology*, 68:2340 – 2349, 2008.
- [3] E. Wilkinson, T.V. Parry, and A.S. Wronski. Compressive failure in two types of carbon fibre-epoxide laminates. *Composites Science and Technology*, 26:17–29, 1986.
- [4] M. Karayaka and P. Kurath. Deformation and failure behavior of woven composite laminates. *Journal of Engineering Materials and Technology (Transactions of the ASME) (USA)*, 116:222–232, 1994.
- [5] A.L. Gyekenyesi. Isothermal fatigue, damage accumulation, and life prediction of a woven pmc. Technical report, NASA/CR-1998-206593, March 1998.
- [6] J.A. Grape and V. Gupta. The effect of temperature on the strength and failure mechanisms of a woven carbon/polyimide laminate under compression. *Mechanics of Materials*, 30(3):165–180, November 1998.
- [7] A.S. Khan, O.U. Colak, and P. Centala. Compressive failure strengths and modes of woven s2-glass reinforced polyester due to quasi-static and dynamic loading. *International Journal of Plasticity*, 18(10):1337–1357, October 2002.
- [8] J. D. McGee and S. Nemat-Nasser. Dynamic bi-axial testing of woven composites. *Materials Science and Engineering A*, 317(1-2):135–139, October 2001.

- [9] F. Mirzadeh and K.L. Reifsnider. Micro-Deformations in C3000/PMR15 Woven Composite. *Journal of Composite Materials*, 26(2):185–205, 1992.
- [10] K.B. Breiling and D.O. Adams. Effects of layer nesting on compression-loaded 2-d woven textile composites. *Journal of Composite Materials*, 30(15):1710–1728, October 1996.
- [11] N. K. Naik and V. K. Ganesh. Failure behavior of plain weave fabric laminates under on-axis uniaxial tensile loading: I-analytical predictions. *Journal of Composite Materials*, 30(16):1779–1822, 1996.
- [12] R.D. Hale and M. Villa. Influence of opposing wave nesting in compression-loaded composites. *Journal of Composite Materials*, 37:1149–1166, 2003.
- [13] D.S. Ivanov, S.V. Lomov, S.G. Ivanov, and I. Verpoest. Stress distribution in outer and inner plies of textile laminates and novel boundary conditions for unit cell analysis. *Composites: Part A*, 41:571–580, 2010.
- [14] R. Gutkin, S.T. Pinho, P. Robinson, and P.T. Curtis. On the transition from shear-driven fibre compressive failure to fibre kinking in notched cfrp laminates under longitudinal compression, accepted for publication in composites science and technology. *Composites Science and Technology*, 70:1223–1231, 2010.
- [15] ASTM standard D 7264/D 7264M - 07, standard test method for flexural properties of polymer matrix composite materials.
- [16] *Physical Acoustic Corporation. PCI-2 based AE system, user's manual*, 2004.
- [17] S.T. Pinho, P. Robinson, and L. Iannucci. Fracture toughness of the tensile and compressive fibre failure modes in laminated composites. *Composites Science and Technology*, 66(13):2069 – 2079, 2006.
- [18] S. Pimenta, R. Gutkin, S.T. Pinho, and P. Robinson. A micromechanical model for kink-band formation: Part II–analytical modelling. *Composites Science and Technology*, 69(7-8):956 – 964, 2009. ISSN 0266-3538.